Andreev transport through single-molecule magnets

F. Pawlicki* and I. Weymann†
Faculty of Physics, Adam Mickiewicz University, ul. Umultowska 85, 61-614 Poznań, Poland

(Received 26 March 2018; published 7 August 2018)

The Andreev transport through a large-spin magnetic molecule, such as a single molecular magnet, attached to superconducting and ferromagnetic leads is studied theoretically by means of the real-time diagrammatic technique. It is shown that due to the proximity effect, molecular Andreev bound states form in the system, with energies depending on the intrinsic parameters of the molecule. We study the spin-resolved Andreev current, conductance, and tunnel magnetoresistance in both the linear and nonlinear response regimes and find regions of negative differential conductance, as well as either enhanced or negative tunnel magnetoresistance. The mechanisms leading to those effects are thoroughly discussed. It is also shown that the tunnel magnetoresistance can provide information about particular spin multiplets responsible for the Andreev reflection processes.

DOI: 10.1103/PhysRevB.98.085411

I. INTRODUCTION

Coupling of a magnetic impurity to a superconductor results in the formation of bound states inside the superconducting energy gap Δ, predicted and studied already half a century ago [1–3]. Such bound states can be, for example, revealed in scanning tunneling spectroscopy experiments for magnetic adatoms deposited on superconducting substrates [4–8]. The bound states can be also examined in tunnel junctions involving a quantum dot or a molecule attached to external superconducting leads [9]. For bias voltages and temperatures lower than Δ, transport in these systems occurs due to the Andreev reflection processes [10]. In fact, Andreev reflection spectroscopy has been recently used to study the Andreev bound states in various nanoscale systems, involving both single and double quantum dots [11–17].

Besides the possibility of exploring the subgap states, hybrid multiterminal nanostructures, involving superconducting and normal electrodes, provide a controllable platform for extracting and manipulating the Cooper pairs in crossed Andreev reflection (CAR) processes [18–21]. In a CAR process the Cooper pair electrons are split into different electrodes, which is opposite to direct Andreev reflection (DAR), where the two electrons tunnel to the same lead. Because controllable extraction and manipulation of entangled electrons is crucial for solid-state quantum computation, a large endeavor has been undertaken to optimize the splitting efficiency of various hybrid devices [22–24]. In addition, it has been also suggested that spin-polarized contacts can play an important role in the detection of entangled electrons [25]. From this point of view, understanding the Andreev transport properties of hybrid nanostructures involving both superconducting and ferromagnetic electrodes is very important. In fact, transport characteristics of such hybrid quantum dot systems have already been a subject of extensive investigations [26–34].

In turn, when instead of a simple spin one-half magnetic impurity a large-spin molecule is embedded in a hybrid tunnel junction, one can expect that additional effects, resulting from intrinsic properties of the molecule, will emerge [35–38]. It is worth mentioning that transport through large-spin molecules, such as single molecular magnets [39], is undergoing an extensive exploration, and the properties of molecular systems with both nonmagnetic and ferromagnetic contacts have been thoroughly analyzed [40–59]. This research has also been stimulated by potential applications, for example, in molecular spintronics and information storage and processing technologies [60,61]. In this context, however, the transport characteristics of magnetic molecules attached to both superconducting and normal (ferromagnetic) leads have been rather poorly studied so far. Only very recently an experimental realization of an artificial molecule composed of coupled quantum dots attached to nonmagnetic and superconducting leads has been reported, where the Yu-Shiba-Rusinov screening of spin triplet states has been observed [62]. The goal of this paper is therefore to shed more light on transport properties of hybrid large-spin molecules and examine the Andreev reflection processes of such molecules attached to ferromagnetic and superconducting electrodes. Our work is thus expected to bring further insight to the interplay of spin-resolved tunneling through large-spin molecules and superconducting proximity-induced effects, paving the way towards further development of superconducting molecular spintronics.

To perform the analysis, we make use of the diagrammatic technique in real time [63], assuming a weak coupling between the molecule and the ferromagnetic leads, while imposing no restriction on the strength of coupling to the superconductor. Moreover, to focus exclusively on Andreev transport and the corresponding subgap states, the analysis is performed in the so-called superconducting atomic limit [64,65], in which the proximity effect is included via a pairing potential induced in the molecule. This pairing results in the formation of molecular Andreev bound states. We resolve those states by studying the bias voltage and the molecule's orbital level dependence of the Andreev current, differential conductance,

*filemon.pawlicki@gmail.com
†weymann@amu.edu.pl

and the tunnel magnetoresistance, which is associated with different magnetic configurations of the device. We show that Andreev reflection processes strongly depend on the intrinsic properties of the molecule, giving rise to enhanced magnetoresistive properties of the device and, depending on the transport regime, negative differential conductance. In addition, in certain transport regimes we find inverse tunnel magnetoresistance of the system. These effects are explained by invoking the nonequilibrium spin accumulation that builds up in the molecule and examining particular Andreev bound states relevant for transport. Furthermore, because large values of tunnel magnetoresistance can be associated with the enhanced role of CAR processes in Andreev reflection [27], our analysis reveals transport regions where crossed Andreev reflection processes are considerable.

The structure of this paper is as follows. The theoretical formulation of the model and method is given in Sec. II, where also the analytical formulas for the molecular Andreev bound states are given. Section III is devoted to presentation and discussion of the numerical results, where we separately analyze the case of nonmagnetic and ferromagnetic leads. Finally, the paper is summarized in Sec. IV.

II. THEORETICAL FORMULATION

A. Model

In this paper we consider a large-spin magnetic molecule, such as a single molecular magnet (SMM), coupled to two ferromagnetic (FM) and one superconducting (SC) lead, as shown schematically in Fig. 1. The magnetizations of the ferromagnetic leads are assumed to be collinear, parallel to the magnetic easy axis of the molecule (z axis), and the configuration of the leads can be either parallel or antiparallel. We assume the electronic transport through the molecule to take place only via the lowest unoccupied molecular orbital (LUMO) of the molecule, which is directly coupled to ferromagnetic and superconducting leads. This orbital level is also coupled to the magnetic core of the molecule via the exchange interaction J. Taking the above into account, the model Hamiltonian assumes the following form:

$$H = H_{\mathrm{SMM}} + \sum_{\beta=L,R} H_\beta + H_S + \sum_{\beta=L,R} H_T^\beta + H_T^S. \quad (1)$$

The first term describes the single molecular magnet in the giant-spin approximation [42,43,46,47,51,56,66]:

$$H_{\mathrm{SMM}} = \sum_\sigma \varepsilon d_\sigma^\dagger d_\sigma + U d_\uparrow^\dagger d_\uparrow d_\downarrow^\dagger d_\downarrow - D S_z^2 - J\boldsymbol{s}\cdot\boldsymbol{S}, \quad (2)$$

where the first two terms describe the LUMO level of energy ε and the Coulomb interaction U between the two electrons occupying that level. The operator $d_\sigma^\dagger$ (d_σ) is a creation (annihilation) operator for an electron in the LUMO level. The third term of H_{SMM} describes the magnetic anisotropy of the molecule, with D being the uniaxial anisotropy constant and S_z is the zth component of the SMM's core spin operator $\boldsymbol{S}$. The last term describes the exchange interaction between the molecule and the LUMO level, where J is an exchange integral. In particular, expressing the local spin operator in terms of electronic creation/annihilation operators, $\boldsymbol{s} = \frac{1}{2}\sum_{\sigma\sigma'} d_\sigma^\dagger \boldsymbol{\sigma}_{\sigma\sigma'} d_{\sigma'}$, where $\boldsymbol{\sigma}_{\sigma\sigma'}$ is a matrix element of the vector of Pauli spin matrices, we can rewrite the last term explicitly as

$$J\boldsymbol{s}\cdot\boldsymbol{S} = \frac{J}{2} d_\uparrow^\dagger d_\downarrow S_- + \frac{J}{2} d_\downarrow^\dagger d_\uparrow S_+ + \frac{J}{2}(d_\uparrow^\dagger d_\uparrow - d_\downarrow^\dagger d_\downarrow) S_z. \quad (3)$$

The exchange interaction can be either of ferromagnetic ($J > 0$) or antiferromagnetic ($J < 0$) type [47], and in the following sections we will treat both cases separately. In these considerations we neglect corrections to the magnitude of the uniaxial anisotropy due to the charging of the LUMO level. These corrections are typically much smaller than the anisotropy constant itself and their effect is relatively small and mainly quantitative [47]. We also consider only one orbital level of the molecule to be relevant for transport. This is motivated by experimental data where typically Coulomb diamonds associated with charging of a single orbital level are observed [39,40,56].

The second term of the total Hamiltonian describes the left ($\beta = L$) and right ($\beta = R$) ferromagnetic electrode in the noninteracting electron gas approximation, characterized by the dispersion relation $\varepsilon_{\boldsymbol{k}\beta\sigma}$, where σ is a spin index and $\boldsymbol{k}$ is an electron wave vector. The explicit form of this term is

$$H_\beta = \sum_{\boldsymbol{k}\sigma} \varepsilon_{\boldsymbol{k}\beta\sigma} c_{\boldsymbol{k}\beta\sigma}^\dagger c_{\boldsymbol{k}\beta\sigma}, \quad (4)$$

where $c_{\boldsymbol{k}\beta\sigma}^\dagger$ ($c_{\boldsymbol{k}\beta\sigma}$) is the corresponding creation (annihilation) operator. The third term in Eq. (1) describes the s-wave BCS superconducting lead in the mean-field approximation,

$$H_S = \sum_{\boldsymbol{k}\sigma} \varepsilon_{\boldsymbol{k}S} c_{\boldsymbol{k}S\sigma}^\dagger c_{\boldsymbol{k}S\sigma} + \sum_{\boldsymbol{k}} \Delta(c_{\boldsymbol{k}S\downarrow} c_{-\boldsymbol{k}S\uparrow} + c_{-\boldsymbol{k}S\uparrow}^\dagger c_{\boldsymbol{k}S\downarrow}^\dagger), \quad (5)$$

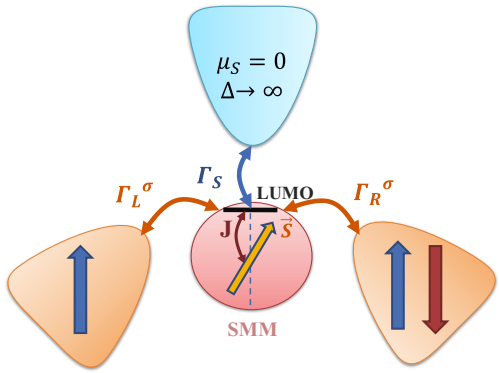

FIG. 1. Schematic of the system under consideration. The magnetic molecule is attached to an s-wave superconductor with coupling strength Γ_S and to ferromagnetic leads with spin-dependent couplings, Γ_L^σ and Γ_R^σ, respectively. Transport occurs due to tunneling through the lowest unoccupied molecular orbital (LUMO) of the molecule, which is exchange-coupled (with exchange interaction J) to the magnetic core spin $\boldsymbol{S}$ of the molecule. The magnetizations of the ferromagnetic leads can be either parallel or antiparallel. The case of infinite superconducting gap $\Delta \to \infty$ is considered. The chemical potential of the superconductor is set to zero.

where $\varepsilon_{\boldsymbol{k}S}$ denotes the single-particle energy and Δ is the superconducting order parameter, which is assumed to be real and momentum-independent.

Finally, the last two terms of the total Hamiltonian describe the tunneling processes between the molecule and external leads. For normal and superconducting leads these are given by

$$H_T^\beta = \sum_{\boldsymbol{k}\sigma} V_{\boldsymbol{k}\beta\sigma}(c^\dagger_{\boldsymbol{k}\beta\sigma} d_\sigma + \text{H.c.}) \tag{6}$$

and

$$H_T^S = \sum_{\boldsymbol{k}\sigma} V_{\boldsymbol{k}S}(c^\dagger_{\boldsymbol{k}S\sigma} d_\sigma + \text{H.c.}), \tag{7}$$

respectively, where $V_{\boldsymbol{k}\beta\sigma}$ ($V_{\boldsymbol{k}S}$) are the relevant tunneling amplitudes between the molecule and the corresponding lead β (superconductor). In the following we assume that the tunneling amplitudes are momentum-independent, $V_{\boldsymbol{k}\beta\sigma} \equiv V_{\beta\sigma}$ and $V_{\boldsymbol{k}S} \equiv V_S$. The coupling of the molecule to the ferromagnetic leads can be parametrized by $\Gamma^\sigma_\beta = 2\pi|V_{\beta\sigma}|^2\rho^\sigma_\beta$, where ρ^σ_β denotes the density of states of the ferromagnetic lead β ($\beta = L, R$) for spin σ. The couplings can be also expressed in terms of spin polarization p_β of the lead β as $\Gamma^\sigma_\beta = \Gamma_\beta(1 + \hat{\sigma}\, p_\beta)$, where $\hat{\sigma} = 1$ ($\hat{\sigma} = -1$) for the coupling to the majority-spin (minority-spin) subband of ferromagnetic lead β. The spin polarization of lead β is defined as $p_\beta = (\rho^+_\beta - \rho^-_\beta)/(\rho^+_\beta + \rho^-_\beta)$, where ρ^+_β (ρ^-_β) is the density of states of the corresponding majority (minority) spin band. Here, we assume symmetric couplings to ferromagnetic leads, $\Gamma_L = \Gamma_R \equiv \Gamma/2$, and symmetric, collinear lead polarizations, $p_L = p_R \equiv p$.

B. Effective SMM-SC Hamiltonian and molecular Andreev bound states

In our considerations we focus on the Andreev reflection regime, therefore, to exclude quasiparticle tunneling in the following we assume that the superconducting energy gap is the largest energy scale in the problem. From the experimental side, this approximation is justified in the low-bias voltage regime, i.e., when the applied bias is smaller than the gap, such that the Andreev levels can be resolved in transport [12,15]. On the other hand, from the theoretical side, it allows us to explore and understand the pure Andreev reflection regime [27,28,30,32–34,67]. In the limit of $\Delta \to \infty$, the molecule coupled to the superconductor, described by $H_{\text{SMM}} + H_S + H_T^S$, can be modeled by the following effective Hamiltonian

$$H^{\text{eff}}_{\text{SMM}} = H_{\text{SMM}} - \frac{\Gamma_S}{2}(d^\dagger_\uparrow d^\dagger_\downarrow + d_\downarrow d_\uparrow), \tag{8}$$

with the last term corresponding to the proximity-effect-induced pairing potential [30,64,65] in the molecule. Here, $\Gamma_S = 2\pi|V_S|^2\rho_S$ is the coupling strength between the superconducting lead and the magnetic molecule, where ρ_S denotes the density of states of the superconductor in the normal state.

Let us start the discussion by analyzing the spectrum of the effective SMM-SC Hamiltonian. The local states of the LUMO level are the following, $|\alpha\rangle_{\text{L}} = \{|0\rangle_{\text{L}}, |\uparrow\rangle_{\text{L}}, |\downarrow\rangle_{\text{L}}, |2\rangle_{\text{L}}\}$, for the empty, singly occupied with spin-up/spin-down electron, and doubly occupied level. On the other hand, the local states of the magnetic core of the molecule can be denoted by the spin S and its zth component quantum numbers, $|S, S_z\rangle_{\text{core}}$. The local state of the effective Hamiltonian can be thus written as a tensor product of the LUMO level state and the state of the internal magnetic core of the molecule, $|\alpha, S, S_z\rangle = |S, S_z\rangle_{\text{core}} \otimes |\alpha\rangle_{\text{L}}$. However, these states are not the eigenstates of $H^{\text{eff}}_{\text{SMM}}$. This is due to the exchange coupling J, which mixes the spin subspaces of the LUMO level and the molecule's core spin, and the pairing correlations, which do not conserve charge. Nevertheless, because the pairing correlations conserve the charge parity and the total spin, $S_{\text{tot}} = S + s$, one can immediately infer that the eigenstates in the case of singly occupied LUMO level are the same as for $\Gamma_S = 0$ and can be found, e.g., in Ref. [47]. We label these states as $|S_{\text{tot}}, S^z_{\text{tot}}\rangle_o$, where subscript indicates that the occupancy of the LUMO level is odd. On the other hand, the empty and doubly occupied LUMO states are mixed due to particle-nonconserving proximity-induced terms of the effective Hamiltonian, such that the eigenstates in the even (e) LUMO occupation sector become

$$|S_{\text{tot}}, S^z_{\text{tot}}\rangle^\pm_e = \sqrt{\frac{1}{2} \mp \frac{\delta}{4\varepsilon_A}}|0, S, S_z\rangle \mp \sqrt{\frac{1}{2} \pm \frac{\delta}{4\varepsilon_A}}|2, S, S_z\rangle. \tag{9}$$

Here, $\delta = 2\varepsilon + U$ denotes the detuning from the particle-hole symmetry point, $\varepsilon = -U/2$, and $2\varepsilon_A = \sqrt{\delta^2 + \Gamma_S^2}$ is the energy difference between the states $|S_{\text{tot}}, S^z_{\text{tot}}\rangle^+_e$ and $|S_{\text{tot}}, S^z_{\text{tot}}\rangle^-_e$. Clearly, for uniaxial magnetic anisotropy $D > 0$ as considered here, the ground state is twofold degenerate and given by $|S^z_{\text{tot}}| = S_{\text{tot}}$. Note also that in the even occupation sector $S_{\text{tot}} = S$ and $S^z_{\text{tot}} = S_z$. The eigenenergies of the above states are given by

$$E^\pm_e = \frac{\delta}{2} \pm \varepsilon_A - DS^2 \tag{10}$$

and they do not depend on the type of exchange interaction J.

The excitation energies between the odd and even states can be used to determine the energies of the Andreev bound states (ABS). In principle, there is a finite probability of excitations between various even and odd molecular states. In practice, however, the highest contribution to transport comes from the transitions involving the two even states $|S_{\text{tot}}, S^z_{\text{tot}}\rangle^\pm_e$ and the odd states representing the lowest-energy components of the multiplets with $S_{\text{tot}} = S + \frac{1}{2}$ and $S_{\text{tot}} = S - \frac{1}{2}$. Because the multiplet which is the ground state in the odd occupation regime depends on the type of exchange interaction, let us discuss these two cases separately. Moreover, we recall that in the absence of magnetic field, as considered in this paper, the spin states are twofold degenerate; however, for the sake of clarity, we will analyze only the positive-spin components.

For the ferromagnetic exchange interaction ($J > 0$), the ground state (GS) in the odd-parity sector is explicitly given by $|S_{\text{tot}} = S + \frac{1}{2}, S^z_{\text{tot}} = S + \frac{1}{2}\rangle^{\text{FM}}_{o,GS} = |\uparrow, S, S_z\rangle$, and has the energy

$$E^{\text{FM}}_{o,GS} = \varepsilon - DS^2 - \frac{JS}{2}. \tag{11}$$

On the other hand, the lowest-energy state of the multiplet with $S_{\text{tot}} = S - \frac{1}{2}$ is a superposition of the states $|\uparrow, S, S-1\rangle$ and

$|\downarrow, S, S\rangle$ [47], while its energy is given by

$$E^{\mathrm{FM}}_{o,exc} = \varepsilon - DS^2 + \frac{J}{4} + D\left(S - \frac{1}{2}\right) + \Delta, \tag{12}$$

where $\Delta = \frac{1}{4}[4D(D-J)(2S-1)^2 + J^2(2S+1)^2]^{1/2}$. Thus, one can distinguish two sets of Andreev bound state energies ($\mathcal{E}$), which are explicitly given by

$$\mathcal{E}^{\mathrm{FM}}_{\alpha\beta} = \alpha\frac{U + JS}{2} + \beta\varepsilon_A \tag{13}$$

and

$$\mathcal{E}^{\mathrm{FM}}_{\mathrm{exc},\alpha\beta} = \alpha\frac{2U - J - 2D(2S-1) - 4\Delta}{4} + \beta\varepsilon_A, \tag{14}$$

where $\alpha, \beta = +, -$. The first four states, $\mathcal{E}^{\mathrm{FM}}_{\alpha\beta}$, are associated with excitations between the two even states, cf. Eq. (9), and the odd-parity ground states, whereas the four additional states, $\mathcal{E}^{\mathrm{FM}}_{\mathrm{exc},\alpha\beta}$, are due to excitations between the same even states and the excited spin multiplet $S_{\mathrm{tot}} = S - \frac{1}{2}$. For $\alpha = +$, the ABS states correspond to the excitations from the odd to the even states, while the states with $\alpha = -$ are related to the opposite transitions.

On the other hand, for the antiferromagnetic exchange coupling ($J < 0$), the role of the above discussed ground and excited states in the odd-parity regime is generally reversed. Now, the ground state becomes the multiplet with $S_{\mathrm{tot}} = S - \frac{1}{2}$ and its energy is given by

$$E^{\mathrm{AFM}}_{o,GS} = \varepsilon - DS^2 - \frac{|J|}{4} + D\left(S - \frac{1}{2}\right) - \Delta, \tag{15}$$

while the energy of the relevant excited state, i.e., the multiplet with $S_{\mathrm{tot}} = S + \frac{1}{2}$, reads

$$E^{\mathrm{AFM}}_{o,exc} = \varepsilon - DS^2 + \frac{|J|S}{2}. \tag{16}$$

This yields the following Andreev bound state energies,

$$\mathcal{E}^{\mathrm{AFM}}_{\alpha\beta} = \alpha\frac{2U + |J| - 2D(2S-1) + 4\Delta}{4} + \beta\varepsilon_A, \tag{17}$$

and four others due to tunneling through excited odd states,

$$\mathcal{E}^{\mathrm{AFM}}_{\mathrm{exc},\alpha\beta} = \alpha\frac{U - |J|S}{2} + \beta\varepsilon_A, \tag{18}$$

with $\alpha, \beta = +, -$.

By comparing the two cases of ferromagnetic and antiferromagnetic exchange coupling, one can note some similarities between the energies of Andreev bound states. As one could expect, the main difference in the above formulas is the sign change of J. However, there is also a more subtle point that needs to be emphasized. While for $J > 0$, the energies $\mathcal{E}^{\mathrm{FM}}_{\alpha\beta}$ correspond to excitations between even states and the odd ground state of the effective Hamiltonian, for $J < 0$, the corresponding energies $\mathcal{E}^{\mathrm{AFM}}_{\mathrm{exc},\alpha\beta}$ result from transitions between respective excited states. This difference will be reflected in the behavior of the Andreev current and the associated differential conductance, as shown in the sequel, since the Andreev bound states resulting from the lowest-energy excitations will be much more pronounced compared to the other ABS states.

We also note that the formulas for the molecular Andreev bound states presented above are quite general and hold for an arbitrary molecule's spin S within the giant spin approximation, in which the molecule is described by its ground-state spin multiplet. Such approximation has been frequently used in the literature [42,43,51,56,66], and is justified for the low-energy physics considered here. The corrections resulting from higher-energy spin multiplets are expected to hardly change the presented results in the studied parameter space.

C. Calculation method

To determine the Andreev current flowing through the considered hybrid molecular system, we employ the real-time diagrammatic technique [63,68,69]. The main idea of this method is a systematic expansion of the reduced density matrix of the system with respect to the coupling strength of the molecule to the ferromagnetic leads Γ. After integrating out the electronic degrees of freedom of ferromagnetic leads, we obtain the reduced density matrix, the time evolution of which essentially determines the transport characteristics of interest. The time evolution can be depicted graphically as a sequence of irreducible diagrams (self-energies) on the Keldysh contour. The self-energy plays a crucial role in the diagrammatic technique, as it can be interpreted as a general transition rate between given states. The self-energies can be calculated in a perturbative scheme, order by order with respect to tunneling processes, using respective diagrammatic rules [63,68,69]. In this paper we have calculated the relevant self-energies up to the first order of expansion. This covers the sequential tunneling regime for processes between the molecule and ferromagnetic leads, while the coupling to superconductor is treated exactly. This assumption is justified in the weak-coupling regime and, as long as $\Gamma \ll T$, it can also give some insight into transport in the Coulomb blockade regime.

In calculations, we assume that the reduced density matrix is diagonal. In general, however, the superpositions of states $|S_{\mathrm{tot}}, S^z_{\mathrm{tot}}\rangle^+_e$ and $|S_{\mathrm{tot}}, S^z_{\mathrm{tot}}\rangle^-_e$ should also be considered. Nevertheless, because in this paper we are only interested in the case of weak coupling to ferromagnetic leads in comparison to the coupling to the superconductor, i.e., $\Gamma_S \gg \Gamma$, one can neglect the off-diagonal terms as they are at least of the order of $O(\Gamma)$, so they become negligible in the weak-coupling regime [28]. In such a case, the diagonal elements of the reduced density matrix can be determined from the following steady-state master equation [63,68]

$$\sum_{\chi'} \Sigma_{\chi,\chi'} P_{\chi'} = 0, \tag{19}$$

where P_χ is the probability of finding the system in a certain state $|\chi\rangle$, which is the eigenstate of $H^{\mathrm{eff}}_{\mathrm{SMM}}$. $\Sigma_{\chi,\chi'}$ is the self-energy corresponding to the transition between the states $|\chi'\rangle$ and $|\chi\rangle$. Once the occupation probabilities of all the states are found, the current flowing through the lead β can be calculated from [63,68]

$$I_\beta = -\frac{ie}{2\hbar}\sum_{\chi\chi'} \Sigma^{I\beta}_{\chi,\chi'} P_{\chi'}, \tag{20}$$

where $\Sigma^{I\beta}_{\chi,\chi'}$ denotes the self-energy that takes into account the number of electrons that tunneled between the molecule and the corresponding lead. The above formula can be used to

determine the currents flowing through both junctions, which then allows us to find the current flowing into the superconducting electrode from the Kirchhoff's law, $I_S = I_L + I_R$.

We would also like to notice that although we take into account only the lowest-order processes between the molecule and normal leads, the coupling to the superconductor is treated exactly. Consequently, within our approximations we are able to resolve both direct and crossed Andreev reflection processes [27,28,30,33,34].

III. RESULTS AND DISCUSSION

In this section we present and discuss the numerical results on the Andreev current, I_S, the associated differential conductance, $G_S \equiv dI_S/dV$, and tunnel magnetoresistance (TMR) of a large-spin magnetic molecule attached to ferromagnetic and superconducting leads; cf. Fig. 1. Because, in the Andreev transport regime, the current in the antiparallel configuration of magnetic moments of ferromagnetic leads is generally larger than that flowing in the parallel configuration, we define the TMR as [27,30]

$$\mathrm{TMR} = \frac{I_S^{AP} - I_S^P}{I_S^P}. \tag{21}$$

Here, I_S^P (I_S^{AP}) is the Andreev current flowing in the parallel (antiparallel) magnetic configuration of the device. Note that this definition is opposite to that typically used for normal electron transport [70,71]. For Andreev processes, the investigations of TMR can give certain insight into the role of direct (DAR) and crossed (CAR) Andreev reflections in transport. DAR is a process in which a Cooper pair leaving the superconductor tunnels to the same ferromagnetic lead, while a CAR process occurs when electrons forming a Cooper pair are split and tunnel to different leads. Changing the sign of the bias voltage results in inverse processes, i.e., a pair of electrons from single lead (different leads) tunnels into the superconductor as a Cooper pair in a DAR (CAR) process. It is important to note that the rates of these processes depend on the couplings to both majority and minority spin subbands. For CAR processes the rate involves the bands of different leads, while for DAR processes the couplings to the same lead are relevant [27,30]. This implies that any change in magnetic configuration of the device should affect the rate of CAR processes, while leaving DAR unaffected. This observation suggests that studying the behavior of the TMR, besides revealing the magnetoresistive properties of the considered device, shall shed more light onto the relative behavior of CAR and DAR processes in the system. Large TMR can indicate that the role of CAR processes is crucial. It is needless to say that CAR processes are of particular interest, because of potential applications of such hybrid nanoscale systems as solid-state sources of spatially separated entangled particles [18,72,73].

In calculations we assume that the bias voltage is applied symmetrically between the ferromagnetic leads and the superconductor, i.e., $\mu_L = \mu_R = eV$, while $\mu_S = 0$. For positive bias voltage $eV > 0$, a pair of electrons tunnels into the superconductor, while for the opposite bias voltage, the Cooper pairs tunnel to ferromagnetic leads. For the considered system, the current changes sign, $I_S \to -I_S$, under the transformation $eV \to -eV$ and $\delta \to -\delta$.

A. The case of nonmagnetic leads

Let us start the discussion with the case of nonmagnetic leads. To reveal the transport features associated with molecular degrees of freedom, we first present the results for the case of $J = 0$, which corresponds to the single-level quantum dot [27,28,30]. This gives us the possibility to explicitly see how the presence of a large-spin molecule affects the Andreev transport characteristics. The bias voltage and level detuning dependence of the Andreev current and the corresponding differential conductance is shown in the left column of Fig. 2. First of all, one can see that in the case of $J = 0$ there are four Andreev bound states visible in transport characteristics, denoted with dashed lines in Figs. 2(a) and 2(b) and given explicitly by Eq. (13) with $J = 0$. Moreover, it is clearly visible that the Andreev current is maximal in the absence of detuning, $\delta = 0$, and becomes suppressed when $|\delta|$ increases. This is due to the fact that the amplitude for Andreev reflection is the largest when the particle-hole symmetry holds. One can also see that the current vanishes for small values of detuning and low bias voltages. In this region, the LUMO level is singly occupied and there are no states in the transport window, such that the current is suppressed. The Andreev current starts flowing when the applied bias exceeds the energy of one of the ABS states. In fact, the energies of those states become degenerate for $|\delta| \approx \sqrt{U^2 - \Gamma_S^2}$ and two resonances are present in the linear response conductance; cf. Fig. 2(b). Furthermore, in the case of $|\delta| \gtrsim \sqrt{U^2 - \Gamma_S^2}$, the range of bias voltage for which the current is suppressed grows proportionally to the absolute value of detuning $|\delta|$. This is due to the fact that in this regime the occupation of the LUMO level is even and the gap between μ_S and the nearest ABS state increases proportionally to the value of the detuning, such that for larger values of $|\delta|$ a larger bias voltage needs to be applied for the Andreev current to flow.

Important information can be also deduced from the Andreev differential conductance spectra shown in Fig. 2(b). Clearly, the conductance peaks coincide with the energies of Andreev bound states estimated analytically. We also notice that differential conductance (and transport characteristics in general) is asymmetric with respect to the bias reversal. Most evidently, one can see that the top conductance peak, i.e., associated with the ABS state $\mathcal{E}_{++}$, vanishes when the detuning is changed from $\delta/U = 2$ to $\delta/U = -2$, while switching the detuning and bias polarization we notice the vanishing of the bottom conductance peak. This is generally due to the fact that for large positive (negative) detuning, when shifting the voltage down (up) there are no states available in the transport window. Nevertheless, it suffices to flip the sign of either detuning or bias voltage to allow for the Andreev transport to reappear.

In the presence of finite exchange interaction J, the Andreev transport behavior becomes generally more complex. Figures 2(c) and 2(d) present the Andreev current and the corresponding differential conductance in the case of ferromagnetic exchange coupling between the LUMO level and the magnetic core of the molecule ($J > 0$). In calculations, without loss of generality, for the molecule's core spin we assumed $S = 2$. One can immediately see that when Andreev reflection processes take place through a large-spin molecule additional steps in the current and the associated conductance

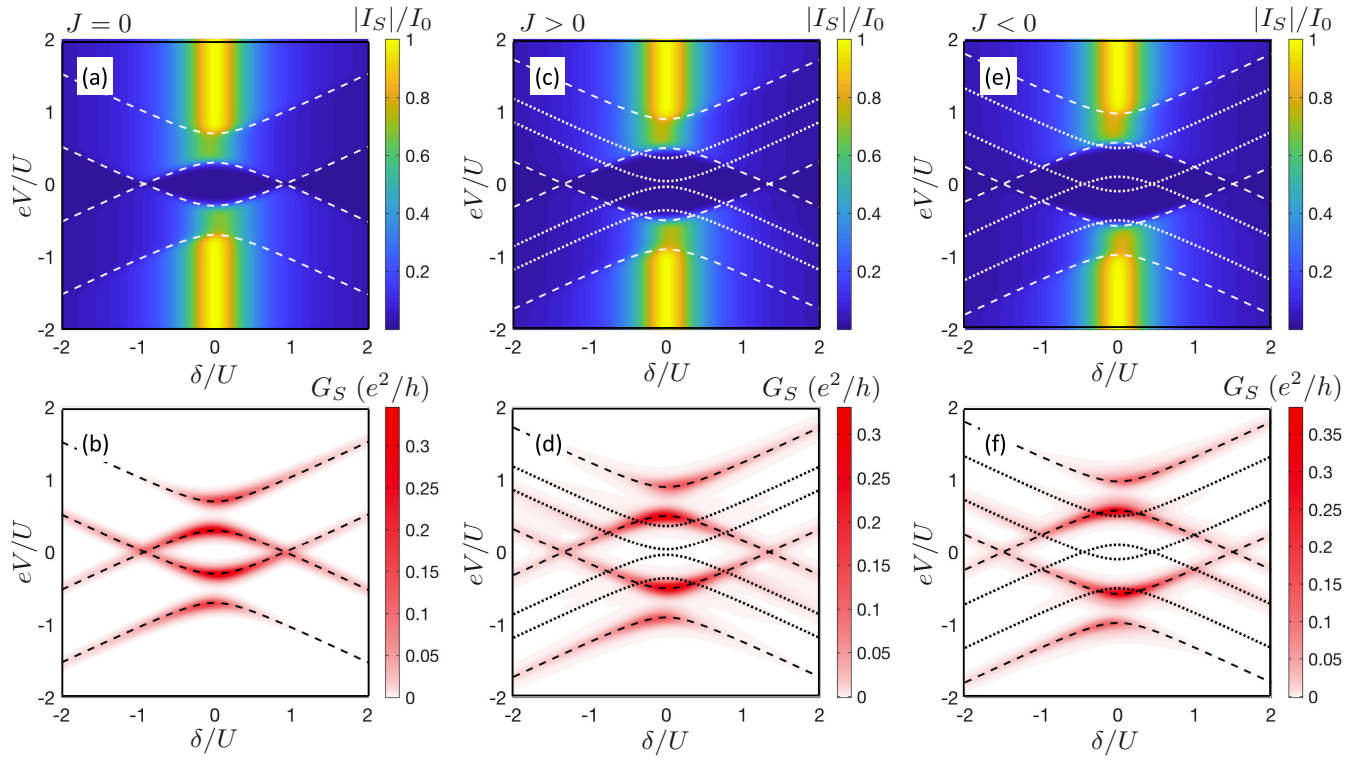

FIG. 2. The Andreev current (first row) and the associated Andreev differential conductance (second row) as a function of the bias voltage eV and the LUMO level detuning $\delta = 2\varepsilon + U$ in the case of (a), (b) $J = 0$, (c), (d) ferromagnetic exchange coupling ($J > 0$) between the LUMO level and the molecule's core spin, and (e), (f) the antiferromagnetic exchange interaction ($J < 0$). The leads are assumed to be nonmagnetic, $p = 0$. The dashed (dotted) lines indicate the energies of Andreev bound states, $\mathcal{E}$ ($\mathcal{E}_{\rm exc}$), derived analytically; see the main text for details. The parameters are $T = 0.03$, $\Gamma_S = 0.4$, $\Gamma = 0.01$, $|J| = 0.2$, $D = 0.05$ in units of $U \equiv 1$, while the spin of the molecule is $S = 2$. The current is plotted in units of $I_0 = e\Gamma/\hbar$.

peaks are present. In fact, these features result from additional ABS states due to excitations between the even and excited odd parity states. The Andreev bound states represented by dashed lines correspond to excitations between the even states and the odd-parity ground state, which are given by Eq. (13). On the other hand, the additional conductance peaks coincide with the Andreev states associated with excitations between even states and highest-weight spin component of the excited multiplet with $S_{\rm tot} = S - \frac{1}{2}$. These are analytically described by Eq. (14). We also note that in the case of $J > 0$ the Andreev linear conductance exhibits two resonances, which now occur for $\delta \approx \pm\sqrt{(U+U)^2 - \Gamma_S^2}$; cf. Fig. 2(d).

The Andreev current and differential conductance in the case of antiferromagnetic exchange coupling ($J < 0$) is presented in Figs. 2(e) and 2(f), respectively. The positions of eight Andreev bound states coinciding with the conductance peaks are given by Eq. (17) (involving the odd-parity ground state) and Eq. (18) (involving odd-parity excited multiplet with $S_{\rm tot} = S + \frac{1}{2}$). Again, a large Coulomb blockade regime can be observed, which is present as long as $|\delta| \lesssim \sqrt{[U + |J|/2 - D(2S-1) + 2\Delta]^2 - \Gamma_S^2}$ and the bias voltage is lower than the corresponding threshold. On the other hand, for larger bias voltages the Andreev conductance exhibits peaks whenever the next ABS state enters the bias window.

As can be seen in Fig. 2, the main difference between the case of a quantum dot ($J = 0$) and a large-spin molecule is the presence of a larger number of Andreev bound states (molecular ABS), which can be resolved in the transport spectroscopy. It is also important to notice that here we focus on molecular ABS that are most pronounced in the differential conductance, i.e., the ones resulting from excitations between even states and the odd states for multiplets $S_{\rm tot} = S + \frac{1}{2}$ and $S_{\rm tot} = S - \frac{1}{2}$, both involving the spin highest-weight components. In general, however, the ABS resulting from the excitations between the other spin components of the odd and even parity sectors may be also present. The amplitude coming from those states is nevertheless relatively small, such that these states are not resolved in Fig. 2, which is due to finite temperature and the fact that the assumed molecule's magnetic anisotropy is not large. Moreover, we would also like to note that the difference between the cases of $J = 0$ and finite J will become much more visible in the spin-resolved Andreev transport properties, since magnetic properties of the molecule will have a profound impact on the Andreev reflection processes. Then, the differences between the cases of ferromagnetic and antiferromagnetic exchange couplings will be also more clearly revealed.

B. The case of ferromagnetic leads

We now proceed to the analysis of the case when the spin polarization of ferromagnetic leads is finite. We set the polarization parameter to $p = 0.5$ and consider the transport characteristics in the parallel and antiparallel magnetic

configuration of the device, as well as its magnetoresistive properties for both the ferromagnetic and antiferromagnetic type of coupling between the LUMO level and the magnetic core of the molecule.

1. Ferromagnetic exchange interaction

Figure 3 presents the bias voltage and the LUMO level detuning dependence of the Andreev differential conductance in the parallel and antiparallel configuration, together with the associated TMR, in the case of ferromagnetic exchange interaction ($J > 0$). In Fig. 3(b) we also explicitly mark the corresponding ABS states. First of all, one can notice that the behavior of the differential conductance in the case of the antiparallel configuration is qualitatively very similar to the nonmagnetic lead case; cf. Figs. 2(d) and 3(b). This is contrary to the situation of the parallel magnetic configuration, where the conductance is found to be generally lower than that in the antiparallel configuration. Moreover, for the parallel configuration some regions with negative differential conductance (NDC) can be observed; see Fig. 3(a). The difference in the behavior of G_S in the two magnetic configurations can be understood as follows. It has already been pointed out that the rate of DAR processes is not affected by the mutual alignment of the two ferromagnets; therefore let us focus on the behavior of CAR processes. For the antiparallel configuration, the Cooper pair electrons, which are involved in a CAR process, always belong to the same subband of the two ferromagnets, i.e., either to the spin majority or to the spin minority subband. Consequently, the two electrons tunnel through the ferromagnetic junctions with the same rates—there is a fast majority and a slow minority spin channel. This is opposite to the case of parallel magnetic configuration, where the two electrons always belong to different subbands. As a consequence, in this case transport is determined by the density of states of the minority band carriers. In fact, in the case of half-metallic leads ($p \to 1$), the Andreev conductance in the parallel configuration becomes fully suppressed due to the lack of minority spin states in the leads. The above mentioned imbalance between the rates of CAR processes in both magnetic configurations explains the observed differences in conductances, i.e., the fact that generally $G_S^{AP} > G_S^{P}$.

However, there are still some transport regions in the case of the parallel configuration, which definitely need further inspection. As one can see in Fig. 3(a), for $\delta > 0$ and positive bias voltage, there are three regimes of negative differential conductance. These can be understood by recalling different rates for tunneling of spin-up and spin-down electrons through the two ferromagnetic junctions. For $\delta \gtrsim \sqrt{(U+U)^2 - \Gamma_S^2}$ and for voltages larger than $\mathcal{E}_{-+}^{\mathrm{FM}}$, i.e., when the first ABS state enters the transport window, there is a drop of the Andreev current and the associated negative differential conductance develops; see Fig. 3(a). This can be also clearly seen in Figs. 4(d) and 4(e), which show the bias dependence of the Andreev current and differential conductance, respectively, calculated for $\delta/U = 2$. In the considered transport regime the LUMO level is empty for $eV \lesssim \mathcal{E}_{-+}^{\mathrm{FM}}$ [$eV \lesssim U/3$ in the inset of Fig. 4(d)] and becomes singly occupied once the bias voltage exceeds the threshold. The LUMO occupation becomes then however strongly spin polarized due to the spin dependence

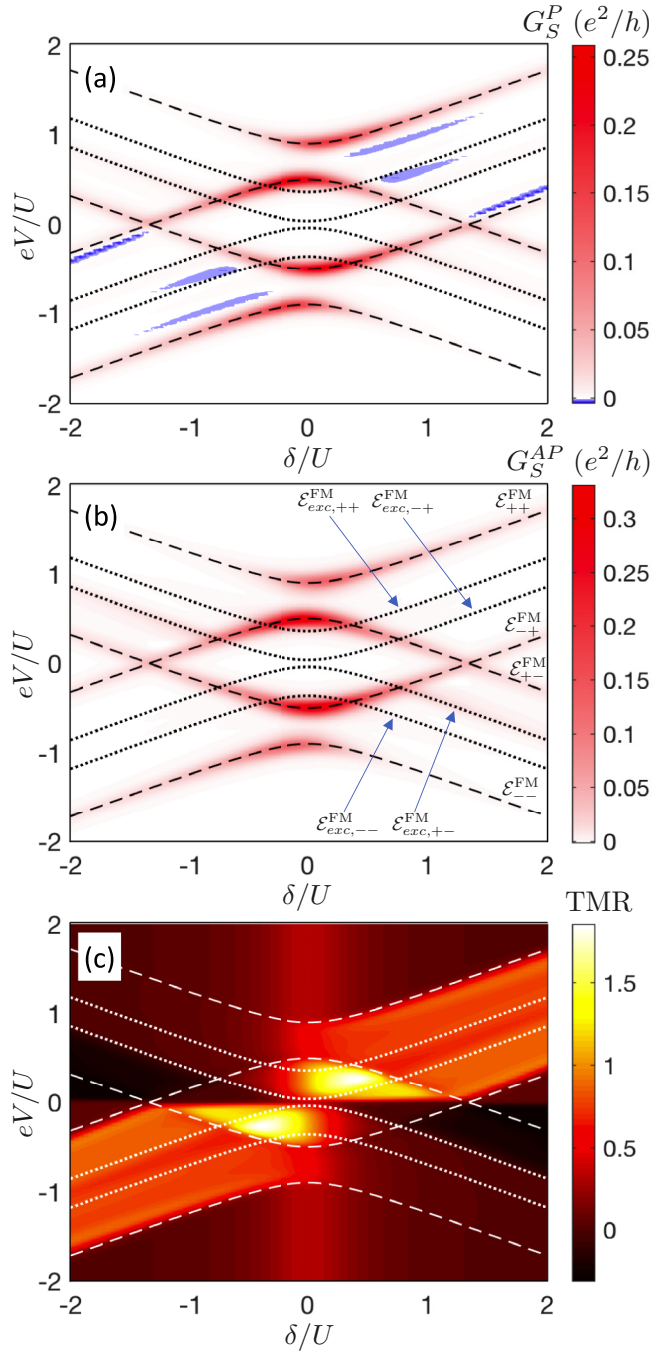

FIG. 3. The Andreev differential conductance in (a) the parallel and (b) antiparallel magnetic configuration as well as (c) the tunnel magnetoresistance plotted as a function of bias voltage eV and the molecule's level detuning δ in the case of ferromagnetic exchange interaction with $J/U = 0.2$. The parameters are the same as in Fig. 2 with $p = 0.5$. The dashed and dotted lines indicate the positions of the corresponding Andreev bound states derived in Sec. II B and given by Eqs. (13) and (14).

of tunneling processes. This is a direct consequence of the fact that the tunnel rate for minority spin electrons is much lower than that of majority spin electrons. As a consequence, a large nonequilibrium spin accumulation develops in the LUMO level (note that the core spin of the molecule is also

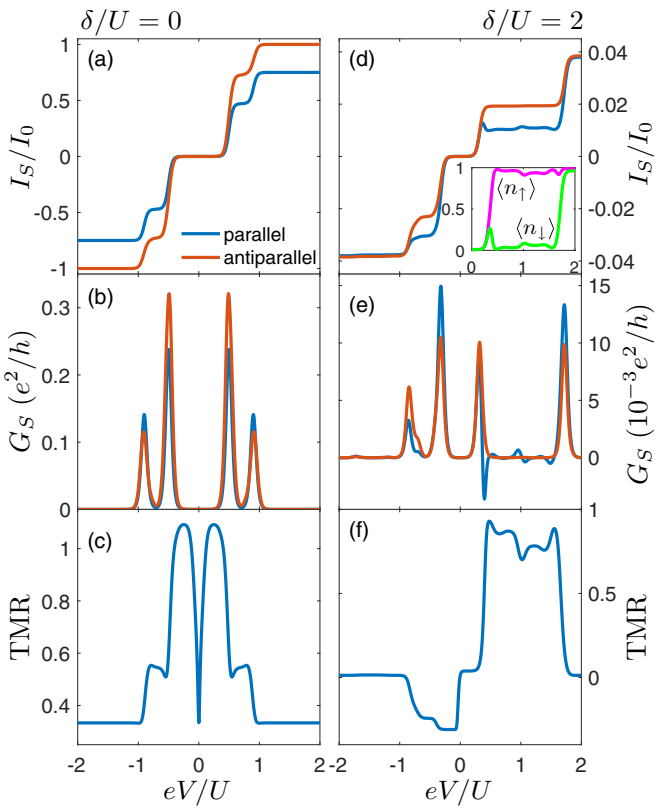

FIG. 4. The bias voltage dependence of (a), (d) the Andreev current, (b), (e) the differential conductance in the parallel and antiparallel configuration, as well as (c), (f) the tunnel magnetoresistance calculated for ferromagnetic exchange interaction. The left column corresponds to $\delta = 0$, while the right column shows the results for $\delta/U = 2$. The inset in (d) presents the expectation values of the spin-resolved LUMO occupation for the parallel configuration and for bias voltages where the negative differential conductance develops. The other parameters are the same as in Fig. 3.

highly spin polarized then). This can be explicitly seen in the inset of Fig. 4(d), which depicts the bias voltage dependence of the spin-resolved LUMO level occupation number $\langle n_\sigma \rangle$ in the case of the parallel magnetic configuration, where $n_\sigma = d_\sigma^\dagger d_\sigma$. Clearly, because the spin-up electrons (belonging to the majority spin subband) can more easily tunnel to the LUMO level, the occupation of this level is much larger for spin-up compared to the spin-down electrons, such that $\langle n_\uparrow \rangle > \langle n_\downarrow \rangle$; see Fig. 4(d). A direct consequence of this fact is the drop of the Andreev current and the associated NDC, because it is now more difficult for the Cooper pair, which involves electrons with opposite spins, to tunnel through the system.

It is also interesting to notice that in the cross section of Fig. 3(a) shown in Fig. 4(e) one can observe other small resonances in the differential conductance, as well as tiny regions of negative differential conductance. These are associated with ABS states due to the other excited states of the molecule. The regions with small NDC are related to the fact that when more ABS states enter the transport window the nonequilibrium spin accumulation in the LUMO level slightly changes [cf. the inset in Fig. 4(d)], and such variations can result in a small current drop.

The other two large negative differential conductance regions can be seen for $\delta/U \approx 1$ in Fig. 3(a). The first one occurs for voltages slightly below the energy of the state $\mathcal{E}^{\rm FM}_{{\rm exc},++}$, while the second one develops for voltages just before the resonance associated with the ABS state $\mathcal{E}^{\rm FM}_{++}$. These NDC regions are again associated with nonequilibrium spin accumulation in the LUMO level, which results in the drop of the Andreev current. Finally, all the regions of negative differential conductance disappear once the occupation of the LUMO level changes again to even, which happens once $eV \gtrsim \mathcal{E}^{\rm FM}_{++}$. Note also that NDC is not present in the case of $\delta = 0$, when the Andreev current is maximized and the electron- and hole-like excitations have the same energy. Then, the transport characteristics are symmetric with respect to the bias reversal. This situation is presented in Figs. 4(a) and 4(b), which show the bias voltage dependence of I_S and G_S in the two magnetic configurations for $\delta = 0$. As already mentioned, the differential conductance spectra are symmetric under the transformation $\delta \to -\delta$ and $eV \to -eV$ and the associated NDC regions visible for $\delta < 0$ and $eV < 0$ in Fig. 3(a) can be understood in a similar fashion by invoking the nonequilibrium spin accumulation in the molecule.

The different behavior of the Andreev reflection processes in the two magnetic configurations of the device is clearly revealed in the tunnel magnetoresistance, the bias voltage and detuning dependence of which is shown in Fig. 3(c). Generally, the TMR is positive in almost entire range of eV and δ. This is due to the fact that, as was explained above, in the antiparallel configuration both electrons forming a Cooper pair belong to the same spin subband, such that there is a fast majority spin channel for Andreev processes and the current is maximized. Interestingly, the values of the TMR are much larger compared to those predicted in the case of $J = 0$ [30], where the TMR was found to be $0 < \text{TMR} < 2p^2/(1-p^2)$. For magnetic molecules we find that the magnetoresistance due to Andreev processes can largely exceed $\text{TMR} = 2p^2/(1-p^2)$ and it can even become negative.

Let us first discuss the mechanisms leading to large TMR. The transport regions where enhanced TMR develops are also presented in the cross sections of Fig. 3(c), which are depicted in Figs. 4(c) and 4(f) and calculated for $\delta = 0$ and $\delta/U = 2$, respectively. In the case of $\delta = 0$, an enhanced TMR develops for voltages around the threshold for sequential processes. The reason for its development is a large spin polarization of the molecule in the parallel magnetic configuration once a finite bias voltage is applied. In fact, one then finds $\langle S_{\rm tot} \rangle \to S^z_{\rm tot}$ for $eV > 0$ and $\langle S_{\rm tot} \rangle \to -S^z_{\rm tot}$ for $eV < 0$ (note that $S_{\rm tot} = S + \frac{1}{2}$). Consequently, the Andreev current in the parallel configuration becomes much suppressed compared to that in the antiparallel configuration, where $\langle S_{\rm tot} \rangle \approx 0$. With increasing the bias voltage $|eV|$, the TMR drops in a two-step-like fashion, see Fig. 4(c), which results from a similar two-step-like decrease of the nonequilibrium spin accumulation. The first step with decreased TMR for $eV > 0$ occurs for $\mathcal{E}^{\rm FM}_{+-} \lesssim eV \lesssim \mathcal{E}^{\rm FM}_{++}$ [for $U/2 \lesssim eV \lesssim U$ in Fig. 4(c)], while for negative bias it takes places when $\mathcal{E}^{\rm FM}_{--} \lesssim eV \lesssim \mathcal{E}^{\rm FM}_{-+}$ [$-U \lesssim eV \lesssim -U/2$]. On the other hand, once $eV \gtrsim \mathcal{E}^{\rm FM}_{++}$ or

$eV \lesssim \mathcal{E}^{\rm FM}_{--}$ [$|eV| \gtrsim U$ in Fig. 4(c)], all the molecular states start contributing to Andreev transport and one then finds TMR $= p^2/(1-p^2)$, which is similar to the quantum dot case [30].

Another region where the TMR is enhanced develops for positive detuning and the bias voltage such that the occupation of the LUMO level is odd ($\mathcal{E}^{\rm FM}_{-+} \lesssim eV \lesssim \mathcal{E}^{\rm FM}_{++}$); see Figs. 3(c) and 4(f). The mechanism responsible for large difference between the Andreev currents flowing in the two magnetic configurations is again associated with nonequilibrium spin accumulation, which builds up in the parallel configuration and suppresses the rate of Andreev processes; see the inset in Fig. 4(d).

Quite counterintuitively, the TMR can also take negative values; see, e.g., Fig. 4(f) in the negative bias voltage range. In this situation, despite the asymmetry in the couplings to ferromagnetic leads, which favors the Andreev current in the antiparallel configuration, the current in the parallel configuration is larger. The mechanism responsible for such behavior is associated with appropriate distribution of the occupation probabilities of the states of the proximized molecule. It turns out that in the parallel magnetic configuration, once the bias voltage becomes negative, the molecule becomes predominantly occupied by the even-parity state $|S,-S\rangle^+_e$. This is contrary to the antiparallel configuration case, where no particular state is so strongly distinguished from the other states. Because the corresponding even state is relevant for driving the Andreev reflection processes, one finds $|I^P_S| > |I^{AP}_S|$ and the associated negative TMR develops. With further increasing the negative bias voltage, the occupation of $|S,-S\rangle^+_e$ in the parallel configuration drops, and negative TMR eventually disappears, such that for $eV \lesssim \mathcal{E}^{\rm FM}_{{\rm exc},+-}$ [$eV \lesssim -U$ in Fig. 4(f)], the TMR becomes generally suppressed. We also note that the region of negative TMR for $\delta > 0$ extends for $\mathcal{E}^{\rm FM}_{{\rm exc},+-} \lesssim eV \lesssim 0$ and a similar behavior is observed for reversed bias voltage and $\delta < 0$; see Fig. 3(c).

2. Antiferromagnetic exchange interaction

Let us now analyze the Andreev transport behavior for the magnetic molecule with antiferromagnetic exchange coupling ($J < 0$). The bias voltage and LUMO level detuning dependence of the differential conductance in both magnetic configurations as well as the TMR is shown in Fig. 5. The dashed and dotted lines present the energies of the corresponding Andreev bound states $\mathcal{E}^{\rm AFM}_{\alpha\beta}$ and $\mathcal{E}^{\rm AFM}_{{\rm exc},\alpha\beta}$, estimated from Eqs. (17) and (18), respectively. The relevant cross sections of this figure are shown in Fig. 6 and present the bias dependence of the current, differential conductance, and TMR for $\delta = 0$ and $\delta/U = 2$. Because the behavior of the differential conductance in the case of the antiparallel configuration is qualitatively similar to the nonmagnetic case, let us focus on the behavior of G^P_S shown in Fig. 5(a).

One can see that for $eV \gtrsim \mathcal{E}^{\rm AFM}_{-+}$ and $\delta/U \gtrsim 1$, G^P_S exhibits a pronounced region of negative differential conductance. This effect again occurs in the transport regime when the occupation of the molecule is odd. For the case of $\delta/U = 2$ presented in the right column of Fig. 6, this happens for $\mathcal{E}^{\rm AFM}_{-+} \lesssim eV \lesssim \mathcal{E}^{\rm AFM}_{++}$, i.e., $U/2 \lesssim eV \lesssim 3U/2$ for assumed parameters. Then, similarly to the case of ferromagnetic exchange interaction, a

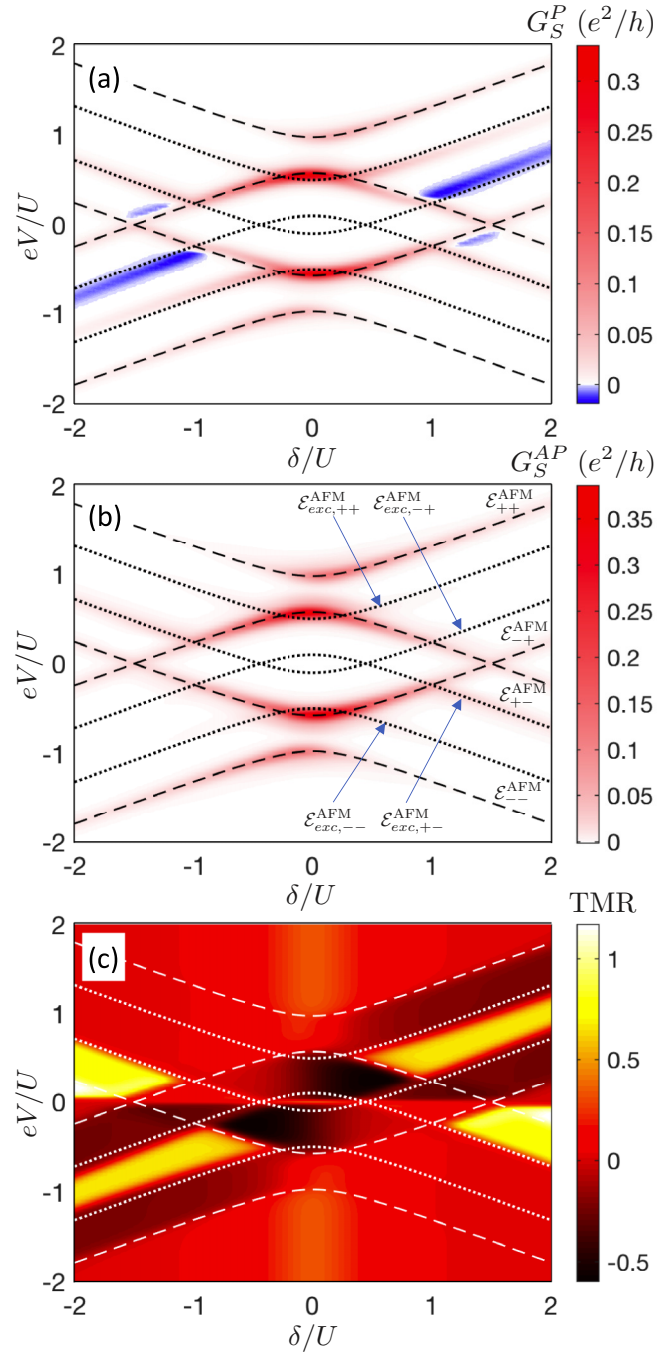

FIG. 5. The Andreev differential conductance in (a) the parallel and (b) antiparallel magnetic configuration and (c) the TMR calculated as a function of eV and δ in the case of antiferromagnetic exchange interaction. The parameters are the same as in Fig. 3 with $J/U = -0.2$. The dashed and dotted lines indicate the positions of the corresponding Andreev bound states derived in Sec. II B and given by Eqs. (17) and (18).

nonequilibrium spin accumulation builds up in the molecule. In the case of $J < 0$, however, depending on the bias voltage, there are certain crucial differences. First of all, the molecule's core spin is highly spin polarized with $\langle S_z\rangle \approx S$ in the whole odd LUMO occupation regime. Interestingly, this is not the case for the spin on the molecule's orbital level, for which

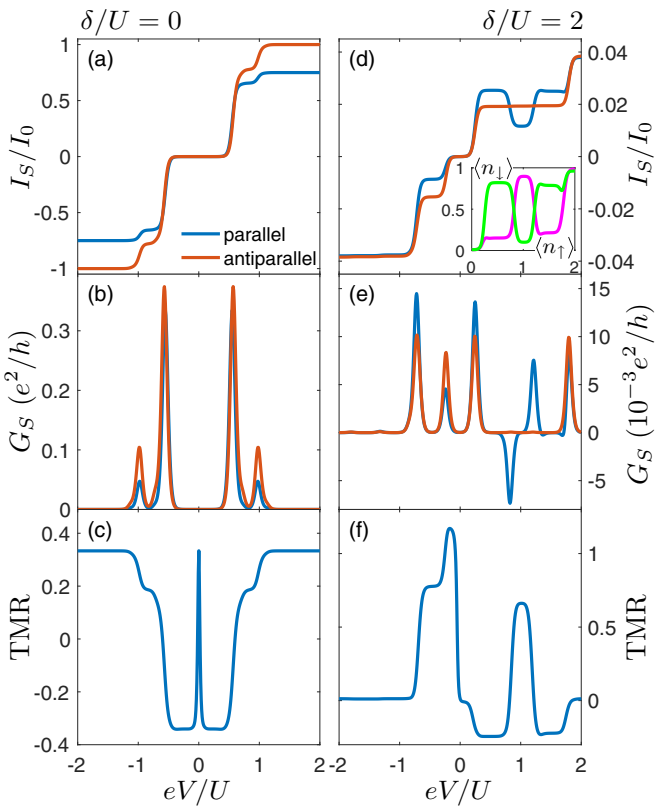

FIG. 6. (a), (d) The Andreev current, (b), (e) differential conductance, and (c), (f) TMR plotted as a function of bias voltage for $\delta = 0$ (left column) and $\delta/U = 2$ (right column). The inset in (d) shows the spin-resolved LUMO occupations for the parallel magnetic configuration and for bias voltages where the negative differential conductance develops. The parameters are the same as in Fig. 5.

we actually find $\langle s_z\rangle \approx \frac{1}{2}$ for voltages falling between the energies of the two excited Andreev bound states, $\mathcal{E}^{\rm AFM}_{\rm exc,-+} \lesssim eV \lesssim \mathcal{E}^{\rm AFM}_{\rm exc,++}$ (corresponding to $4U/5 \lesssim eV \lesssim 6U/5$ for assumed parameters) and $\langle s_z\rangle \approx -\frac{1}{2}$ in the other odd occupation regime; see the inset to Fig. 6(d). Thus, with increasing the bias voltage, first the state $|1, S-\frac{1}{2}, S-\frac{1}{2}\rangle$ becomes mainly occupied, then, at $eV \approx \mathcal{E}^{\rm AFM}_{\rm exc,-+}$ ($eV \approx 4U/5$), the occupation of $|1, S+\frac{1}{2}, S+\frac{1}{2}\rangle$ gets enhanced, and when $eV \approx \mathcal{E}^{\rm AFM}_{\rm exc,++}$ ($eV \approx 6U/5$), again the state $|1, S-\frac{1}{2}, S-\frac{1}{2}\rangle$ starts playing an important role. The crucial difference is that once the highest-weight component of the multiplet $S_{\rm tot} = S+\frac{1}{2}$ becomes relevant, nonequilibrium spin accumulation is maximal and the Andreev tunneling gets suppressed, resulting in a considerable NDC.

The internal structure of the molecular states that are mainly relevant for transport is also nicely revealed in the behavior of the TMR, which is shown in Fig. 5(c). Generally, in all the transport regimes where a strong nonequilibrium spin accumulation in the highest spin multiplies builds up, the Andreev conductance in the parallel configuration gets much suppressed compared to the antiparallel case. As a consequence, one then finds an enhanced tunnel magnetoresistance. In the case of antiferromagnetic exchange coupling, the TMR can however also take negative values in much larger parameter space as compared to the case of $J > 0$; cf. Figs. 3(c) and 5(c). In fact, negative TMR occurs now not only for low bias voltages, but also in transport regimes where a large Andreev current can flow; see Fig. 6(f). The enhancement of I_S^P in comparison to I_S^{AP} results from particular states relevant for transport. It needs to be emphasized that an enhanced occupation of certain molecular states due to the spin accumulation can have both positive and negative impact on the Andreev conductance. (Recall that in the antiparallel configuration all spin components are equally occupied and $\langle S^z_{\rm tot}\rangle = 0$.) If the occupation of the state $|1, S+\frac{1}{2}, S+\frac{1}{2}\rangle$ is large, it results in the suppression of Andreev conductance, since the LUMO level favors one component of the spin. However, this is just opposite to the case when the other multiplet $|1, S-\frac{1}{2}, S-\frac{1}{2}\rangle$ becomes mainly responsible for Andreev transport. Because this state is a superposition of both spin-up and spin-down components, Andreev processes become much enhanced. Moreover, in this particular case one in fact finds that $I_S^{AP} < I_S^P$, which yields negative TMR; see Fig. 6(f).

In addition, a pronounced negative TMR is also found in the case of $\delta = 0$, which is shown in the left column of Fig. 6. Note that this behavior is completely opposite to the ferromagnetic exchange coupling case. Now, despite the fact that the current is symmetric with respect to the bias reversal and there is no NDC [see Figs. 6(a) and 6(b)], the TMR changes sign and becomes negative. This happens for voltages when the system is in the Coulomb blockade regime. Then, in the regime of $\Gamma \ll T$, the current is mediated by thermally activated sequential processes. In the case of $J > 0$ and for parallel magnetic configuration, in this transport regime the molecule was occupied by the state $|1, S+\frac{1}{2}, S+\frac{1}{2}\rangle$, which led to large TMR. In the case of $J < 0$, in turn, the molecule is occupied by $|1, S-\frac{1}{2}, S-\frac{1}{2}\rangle$, and since this state involves superposition of both up and down spin components the Andreev current gets enhanced compared to I_S^{AP}, yielding TMR < 0; see Fig. 6(c).

Finally, we note that the effect of negative TMR is clearly associated with a particular occupation of molecular states that, despite the asymmetry in the couplings to the ferromagnetic leads, enhances the Andreev current in the parallel configuration. However, one needs to keep in mind that with increasing the spin polarization of the leads, the current in the parallel configuration should eventually become suppressed, such that $I_S^{AP} < I_S^P$ will not hold anymore and the TMR will become positive.

IV. SUMMARY

In this paper we have studied the subgap transport through a large-spin magnetic molecule, such as a single molecular magnet, coupled to one superconducting and two ferromagnetic leads. The analysis has been performed by employing the diagrammatic technique in real time and including lowest-order processes between the molecule and ferromagnetic leads, while the coupling to the superconductor was treated exactly. We have determined the bias voltage and the molecule's orbital level detuning dependence of the Andreev current and associated differential conductance, as well as the tunnel magnetoresistance. We have shown that, due to the super-

conducting proximity effect, transport processes take place through molecular Andreev bound states. The energies of those bound states can be estimated from excitation energies between the odd and even charge parity states. For large-spin molecules, as considered in this paper, there are in principle many such states. However, we have shown that the main peaks visible in the Andreev differential conductance are associated with eight ABS states, resulting from excitations between the even states and the highest-weight spin components of the odd states for multiplets with $S_{\rm tot} = S + \frac{1}{2}$ and $S_{\rm tot} = S - \frac{1}{2}$.

Because the ground state properties of the molecule depend strongly on the type of exchange interaction between the molecule's core spin and the spin of electrons occupying the LUMO level, different behavior was found in these two corresponding cases. This difference is in fact clearly revealed in the case of ferromagnetic leads. Then, for both cases of J, we have identified regions of negative differential conductance in the parallel magnetic configuration. The reason for the current suppression and associated NDC is the nonequilibrium spin accumulation that builds up in the molecule. Moreover, we have shown that there is a crucial difference between the cases of ferromagnetic and antiferromagnetic exchange couplings, resulting in a completely different behavior of the TMR. If the spin accumulation develops in the multiplet with $S_{\rm tot} = S - \frac{1}{2}$, as happens in certain transport regimes for $J < 0$, a large negative TMR can develop. On the other hand, in transport regimes when one of the highest-weight components of the multiplet $S_{\rm tot} = S + \frac{1}{2}$ is mainly responsible for Andreev reflection, the Andreev current in the parallel configuration becomes greatly suppressed. This transport regime is characterized by a large positive TMR.

ACKNOWLEDGMENT

This work was supported by the National Science Centre in Poland through Project No. DEC-2013/10/E/ST3/00213.

[1] L. Yu, Bound state in superconductors with paramagnetic impurities, Acta Phys. Sin. **21**, 75 (1965).
[2] Hiroyuki Shiba, Classical spins in superconductors, Prog. Theor. Phys. **40**, 435 (1968).
[3] A. I. Rusinov, Superconductivity near a paramagnetic impurity, Zh. Eksp. Teor. Fiz. **9**, 146 (1968) [JETP Lett. **9**, 85 (1969)].
[4] M. E. Flatté and J. M. Byers, Local Electronic Structure of a Single Magnetic Impurity in a Superconductor, Phys. Rev. Lett. **78**, 3761 (1997).
[5] A. Yazdani, B. A. Jones, C. P. Lutz, M. F. Crommie, and D. M. Eigler, Probing the local effects of magnetic impurities on superconductivity, Science **275**, 1767 (1997).
[6] S.-H. Ji, T. Zhang, Y.-S. Fu, X. Chen, X.-C. Ma, J. Li, W.-H. Duan, J.-F. Jia, and Q.-K. Xue, High-Resolution Scanning Tunneling Spectroscopy of Magnetic Impurity Induced Bound States in the Superconducting Gap of Pb Thin Films, Phys. Rev. Lett. **100**, 226801 (2008).
[7] M. Ruby, F. Pientka, Y. Peng, F. von Oppen, B. W. Heinrich, and K. J. Franke, End States and Subgap Structure in Proximity-Coupled Chains of Magnetic Adatoms, Phys. Rev. Lett. **115**, 197204 (2015).
[8] N. Hatter, B. W. Heinrich, D. Rolf, and K. J. Franke, Scaling of Yu-Shiba-Rusinov energies in the weak-coupling Kondo regime, Nat. Commun. **8**, 2016 (2017).
[9] A. Martin-Rodero and A. Levy Yeyati, Josephson and Andreev transport through quantum dots, Adv. Phys. **60**, 899 (2011).
[10] A. F. Andreev, Thermal conductivity of the intermediate state of superconductors, Zh. Eksp. Teor. Fiz. **46**, 1823 (1964) [Sov. Phys. JETP **19**, 1228 (1964)].
[11] R. S. Deacon, Y. Tanaka, A. Oiwa, R. Sakano, K. Yoshida, K. Shibata, K. Hirakawa, and S. Tarucha, Tunneling Spectroscopy of Andreev Energy Levels in a Quantum Dot Coupled to a Superconductor, Phys. Rev. Lett. **104**, 076805 (2010).
[12] S. De Franceschi, L. Kouwenhoven, C. Schonenberger, and W. Wernsdorfer, Hybrid superconductor-quantum dot devices, Nat. Nanotechnol. **5**, 703 (2010).
[13] T. Dirks, T. L. Hughes, S. Lal, B. Uchoa, Y.-F. Chen, C. Chialvo, P. M. Goldbart, and N. Mason, Transport through Andreev bound states in a graphene quantum dot, Nat. Phys. **7**, 386 (2011).
[14] B.-K. Kim, Y.-H. Ahn, J.-J. Kim, M.-S. Choi, M.-H. Bae, K. Kang, J. S. Lim, R. López, and N. Kim, Transport Measurement of Andreev Bound States in a Kondo-Correlated Quantum Dot, Phys. Rev. Lett. **110**, 076803 (2013).
[15] E. J. H. Lee, X. Jiang, M. Houzet, R. Aguado, C. M. Lieber, and S. De Franceschi, Spin-resolved Andreev levels and parity crossings in hybrid superconductor-semiconductor nanostructures, Nat. Nanotechnol. **9**, 79 (2014).
[16] J. Gramich, A. Baumgartner, and C. Schönenberger, Resonant and Inelastic Andreev Tunneling Observed on a Carbon Nanotube Quantum Dot, Phys. Rev. Lett. **115**, 216801 (2015).
[17] Z. Su, A. B. Tacla, M. Hocevar, D. Car, S. R. Plissard, E. P. A. M. Bakkers, A. J. Daley, D. Pekker, and S. M. Frolov, Andreev molecules in semiconductor nanowire double quantum dots, Nat. Commun. **8**, 585 (2017).
[18] L. Hofstetter, S. Csonka, J. Nygård, and C. Schönenberger, Cooper pair splitter realized in a two-quantum-dot y-junction, Nature (London) **461**, 960 (2009).
[19] L. Hofstetter, S. Csonka, A. Baumgartner, G. Fülöp, S. d'Hollosy, J. Nygård, and C. Schönenberger, Finite-Bias Cooper Pair Splitting, Phys. Rev. Lett. **107**, 136801 (2011).
[20] Z. B. Tan, D. Cox, T. Nieminen, P. Lähteenmäki, D. Golubev, G. B. Lesovik, and P. J. Hakonen, Cooper Pair Splitting by Means of Graphene Quantum Dots, Phys. Rev. Lett. **114**, 096602 (2015).
[21] G. Fülöp, F. Domínguez, S. d'Hollosy, A. Baumgartner, P. Makk, M. H. Madsen, V. A. Guzenko, J. Nygård, C. Schönenberger, A. Levy Yeyati, and S. Csonka, Magnetic Field Tuning and Quantum Interference in a Cooper Pair Splitter, Phys. Rev. Lett. **115**, 227003 (2015).
[22] A. Das, Y. Ronen, M. Heiblum, D. Mahalu, A. V. Kretinin, and H. Shtrikman, High-efficiency Cooper pair splitting demonstrated by two-particle conductance resonance and positive noise cross-correlation, Nat. Commun. **3**, 2169 (2012).
[23] J. Schindele, A. Baumgartner, and C. Schönenberger, Near-Unity Cooper Pair Splitting Efficiency, Phys. Rev. Lett. **109**, 157002 (2012).

[24] G. Fülöp, S. d'Hollosy, A. Baumgartner, P. Makk, V. A. Guzenko, M. H. Madsen, J. Nygård, C. Schönenberger, and S. Csonka, Local electrical tuning of the nonlocal signals in a Cooper pair splitter, Phys. Rev. B **90**, 235412 (2014).

[25] W. Kłobus, A. Grudka, A. Baumgartner, D. Tomaszewski, C. Schönenberger, and J. Martinek, Entanglement witnessing and quantum cryptography with nonideal ferromagnetic detectors, Phys. Rev. B **89**, 125404 (2014).

[26] J.-F. Feng and S.-J. Xiong, Tunneling resonances and Andreev reflection in transport of electrons through a ferromagnetic metal/quantum dot/superconductor system, Phys. Rev. B **67**, 045316 (2003).

[27] D. Futterer, M. Governale, M. G. Pala, and J. König, Nonlocal Andreev transport through an interacting quantum dot, Phys. Rev. B **79**, 054505 (2009).

[28] B. Sothmann, D. Futterer, M. Governale, and J. König, Probing the exchange field of a quantum-dot spin valve by a superconducting lead, Phys. Rev. B **82**, 094514 (2010).

[29] L. Hofstetter, A. Geresdi, M. Aagesen, J. Nygård, C. Schönenberger, and S. Csonka, Ferromagnetic Proximity Effect in a Ferromagnet–Quantum-Dot–Superconductor Device, Phys. Rev. Lett. **104**, 246804 (2010).

[30] I. Weymann and P. Trocha, Superconducting proximity effect and zero-bias anomaly in transport through quantum dots weakly attached to ferromagnetic leads, Phys. Rev. B **89**, 115305 (2014).

[31] P. Trocha and J. Barnaś, Spin-polarized Andreev transport influenced by Coulomb repulsion through a two-quantum-dot system, Phys. Rev. B **89**, 245418 (2014).

[32] K. P. Wójcik and I. Weymann, Proximity effect on spin-dependent conductance and thermopower of correlated quantum dots, Phys. Rev. B **89**, 165303 (2014).

[33] P. Trocha and I. Weymann, Spin-resolved Andreev transport through double-quantum-dot Cooper pair splitters, Phys. Rev. B **91**, 235424 (2015).

[34] K. Wrześniewski, P. Trocha, and I. Weymann, Current cross-correlations in double quantum dot based Cooper pair splitters with ferromagnetic leads, J. Phys.: Condens. Matter **29**, 195302 (2017).

[35] D. Golež, J. Bonča, and R. Žitko, Vibrational Andreev bound states in magnetic molecules, Phys. Rev. B **86**, 085142 (2012).

[36] B. W. Heinrich, L. Braun, J. I. Pascual, and K. J. Franke, Protection of excited spin states by a superconducting energy gap, Nat. Phys. **9**, 765 (2013).

[37] J. Tejada, R. Zarzuela, A. García-Santiago, I. Imaz, J. Espin, D. Maspoch, and E. M. Chudnovsky, Enhanced spin tunneling in a molecular magnet mixed with a superconductor, J. Supercond. Novel Magn. **29**, 1133 (2016).

[38] L. Cornils, A. Kamlapure, L. Zhou, S. Pradhan, A. A. Khajetoorians, J. Fransson, J. Wiebe, and R. Wiesendanger, Spin-Resolved Spectroscopy of the Yu-Shiba-Rusinov States of Individual Atoms, Phys. Rev. Lett. **119**, 197002 (2017).

[39] D. Gatteschi, R. Sessoli, and J. Villain, *Molecular Nanomagnets* (Oxford University Press, New York, 2006).

[40] D. Gatteschi and R. Sessoli, Quantum tunneling of magnetization and related phenomena in molecular materials, Angew. Chem., Int. Ed. **42**, 268 (2003).

[41] H. B. Heersche, Z. de Groot, J. A. Folk, H. S. J. van der Zant, C. Romeike, M. R. Wegewijs, L. Zobbi, D. Barreca, E. Tondello, and A. Cornia, Electron Transport through Single Mn_{12} Molecular Magnets, Phys. Rev. Lett. **96**, 206801 (2006).

[42] F. Elste and C. Timm, Transport through anisotropic magnetic molecules with partially ferromagnetic leads: Spin-charge conversion and negative differential conductance, Phys. Rev. B **73**, 235305 (2006).

[43] C. Timm and F. Elste, Spin amplification, reading, and writing in transport through anisotropic magnetic molecules, Phys. Rev. B **73**, 235304 (2006).

[44] N. J. Tao, Electron transport in molecular junctions, Nat. Nanotechnol. **1**, 173 (2006).

[45] F. Elste and C. Timm, Cotunneling and nonequilibrium magnetization in magnetic molecular monolayers, Phys. Rev. B **75**, 195341 (2007).

[46] M. Misiorny and J. Barnaś, Spin polarized transport through a single-molecule magnet: Current-induced magnetic switching, Phys. Rev. B **76**, 054448 (2007).

[47] M. Misiorny, I. Weymann, and J. Barnaś, Spin effects in transport through single-molecule magnets in the sequential and cotunneling regimes, Phys. Rev. B **79**, 224420 (2009).

[48] F. Delgado, J. J. Palacios, and J. Fernández-Rossier, Spin-Transfer Torque on a Single Magnetic Adatom, Phys. Rev. Lett. **104**, 026601 (2010).

[49] L. Zhu, K. L. Yao, and Z. L. Liu, Molecular spin valve and spin filter composed of single-molecule magnets, Appl. Phys. Lett. **96**, 082115 (2010).

[50] B. Sothmann and J. König, Transport through quantum-dot spin valves containing magnetic impurities, Phys. Rev. B **82**, 245319 (2010).

[51] M. Misiorny, I. Weymann, and J. Barnaś, Interplay of the Kondo Effect and Spin-Polarized Transport in Magnetic Molecules, Adatoms, and Quantum Dots, Phys. Rev. Lett. **106**, 126602 (2011).

[52] N. Bode, L. Arrachea, G. S. Lozano, T. S. Nunner, and F. von Oppen, Current-induced switching in transport through anisotropic magnetic molecules, Phys. Rev. B **85**, 115440 (2012).

[53] Z. Zhang and L. Jiang, Bias voltage induced resistance switching effect in single-molecule magnets' tunneling junction, Nanotechnology **25**, 365201 (2014).

[54] A. Płomińska and I. Weymann, Nontrivial magnetoresistive behavior of a single-wall carbon nanotube with an attached molecular magnet, Phys. Rev. B **92**, 205419 (2015).

[55] N. Gallego-Planas, A. Martín-Rodríguez, and E. Ruiz, Magnetic and transport properties of Fe_4 single-molecule magnets: A theoretical insight, Dalton Trans. **45**, 18867 (2016).

[56] R. Gaudenzi, M. Misiorny, E. Burzurí, M. R. Wegewijs, and H. S. J. van der Zant, Transport mirages in single-molecule devices, J. Chem. Phys. **146**, 092330 (2017).

[57] A. Płomińska, M. Misiorny, and I. Weymann, Spin-resolved dynamical conductance of a correlated large-spin magnetic molecule, Phys. Rev. B **95**, 155446 (2017).

[58] H. Xie, F. Xu, H. Jiao, Q. Wang, and J.-Q. Liang, Efficient spin-current injection in single-molecule magnet junctions, AIP Adv. **8**, 015131 (2018).

[59] A. Płomińska, I. Weymann, and M. Misiorny, Dynamical spin accumulation in large-spin magnetic molecules, Phys. Rev. B **97**, 035415 (2018).

[60] M. N. Leuenberger and D. Loss, Quantum computing in molecular magnets, Nature (London) **410**, 789 (2001).

[61] L. Bogani and W. Wernsdorfer, Molecular spintronics using single-molecule magnets, Nat. Mater. **7**, 179 (2008).

[62] K. Grove-Rasmussen, G. Steffensen, A. Jellinggaard, M. H. Madsen, R. Žitko, J. Paaske, and J. Nygård, Yu-Shiba-Rusinov screening of spins in double quantum dots, Nat. Commun. **9**, 2376 (2018).

[63] H. Schoeller and G. Schön, Mesoscopic quantum transport: Resonant tunneling in the presence of a strong Coulomb interaction, Phys. Rev. B **50**, 18436 (1994).

[64] A. V. Rozhkov and D. P. Arovas, Interacting-impurity Josephson junction: Variational wave functions and slave-boson mean-field theory, Phys. Rev. B **62**, 6687 (2000).

[65] T. Domański, I. Weymann, M. Barańska, and G. Górski, Constructive influence of the induced electron pairing on the Kondo state, Sci. Rep. **6**, 23336 (2016).

[66] M. Misiorny, M. Hell, and M. R. Wegewijs, Spintronic magnetic anisotropy, Nat. Phys. **9**, 801 (2013).

[67] N. Walldorf, C. Padurariu, A.-P. Jauho, and C. Flindt, Electron Waiting Times of a Cooper Pair Splitter, Phys. Rev. Lett. **120**, 087701 (2018).

[68] J. König, J. Schmid, H. Schoeller, and G. Schön, Resonant tunneling through ultrasmall quantum dots: Zero-bias anomalies, magnetic-field dependence, and boson-assisted transport, Phys. Rev. B **54**, 16820 (1996).

[69] A. Thielmann, M. H. Hettler, J. König, and G. Schön, Shot noise in tunneling transport through molecules and quantum dots, Phys. Rev. B **68**, 115105 (2003).

[70] M. Julliere, Tunneling between ferromagnetic films, Phys. Lett. A **54**, 225 (1975).

[71] J. Barnaś and I. Weymann, Spin effects in single-electron tunnelling, J. Phys.: Condens. Matter **20**, 423202 (2008).

[72] B. Ruggiero, P. Delsing, C. Granata, Y. A. Pashkin, and P. Silvestrini, *Quantum Computing in Solid State Systems* (Springer-Verlag, New York, 2006).

[73] D. Ciudad, Superconductivity: Splitting Cooper pairs, Nat. Mater. **14**, 463 (2015).